crystals

MDPI

Article

Fabrication of C/C–SiC–ZrB_2 Ultra-High Temperature Composites through Liquid–Solid Chemical Reaction

Qian Sun [1,2], Huifeng Zhang [1,3], Chuanbing Huang [1,3] and Weigang Zhang [1,2,3,*]

[1] Key Laboratory of Science and Technology on Particle Materials & State Key Laboratory of Multiphase Complex Systems, Institute of Process Engineering, Chinese Academy of Sciences, Beijing 100190, China; sunqian191@ipe.ac.cn (Q.S.); hfzhang@ipe.ac.cn (H.Z.); cbhuang@ipe.ac.cn (C.H.)
[2] School of Chemical Engineering, University of Chinese Academy of Sciences, Beijing 100049, China
[3] Ganjiang Innovation Academy, Chinese Academy of Sciences, Ganzhou 341000, China
* Correspondence: wgzhang@ipe.ac.cn; Tel.: +86-10-8254-4908

Abstract: In this paper, we aimed to improve the oxidation and ablation resistance of carbon fiber-reinforced carbon (CFC) composites at temperatures above 2000 °C. C/C–SiC–ZrB_2 ultra-high temperature ceramic composites were fabricated through a complicated liquid–solid reactive process combining slurry infiltration (SI) and reactive melt infiltration (RMI). A liquid Si–Zr10 eutectic alloy was introduced, at 1600 °C, into porous CFC composites containing two kinds of boride particles (B_4C and ZrB_2, respectively) to form a SiC–ZrB_2 matrix. The effects and mechanism of the introduced B_4C and ZrB_2 particles on the formation reaction and microstructure of the final C/C–SiC–ZrB_2 composites were investigated in detail. It was found that the composite obtained from a C/C–B_4C preform displayed a porous and loose structure, and the formed SiC–ZrB_2 matrix distributed heterogeneously in the composite due to the asynchronous generation of the SiC and ZrB_2 ceramics. However, the C/C–SiC–ZrB_2 composite, prepared from a C/C–ZrB_2 preform, showed a very dense matrix between the fiber bundles, and elongated plate-like ZrB_2 ceramics appeared in the matrix, which were derived from the dissolution–diffusion–precipitation mechanism of the ZrB_2 clusters. The latter composite exhibited a relatively higher ZrB_2 content (9.51%) and bulk density (2.82 g/cm^3), along with lower open porosity (3.43%), which endowed this novel composite with good mechanical properties, including pseudo-plastic fracture behavior.

Keywords: reactive melt infiltration; C/C–SiC–ZrB_2 composites; composition; microstructural evolution; formation mechanism

check for updates

Citation: Sun, Q.; Zhang, H.; Huang, C.; Zhang, W. Fabrication of C/C–SiC–ZrB_2 Ultra-High Temperature Composites through Liquid–Solid Chemical Reaction. *Crystals* **2021**, *11*, 1352. https://doi.org/10.3390/cryst11111352

Academic Editors: Pavel Lukáč and Rohan Galgalikar

Received: 15 October 2021
Accepted: 3 November 2021
Published: 7 November 2021

1. Introduction

Carbon fiber-reinforced carbon (CFC) composites have been widely used in aerospace industries due to their low density and coefficient of thermal expansion, together with their high mechanical strength and excellent thermal shock resistance [1,2]. However, CFC composites are very vulnerable to oxidizing atmospheres over 400 °C, which limits their applications in extreme environments [3]. To effectively enhance the oxidation and ablation resistance of CFC composites at temperatures above 2000 °C, the effects of SiC combined with Zr-based or Hf-based ultra-high temperature ceramics (UHTCs) have been intensively studied [4–6]. Several methods of introducing SiC-UHTC ceramics into CFC composites have been investigated, such as polymer infiltration and pyrolysis (PIP) [7], slurry infiltration (SI) [8], chemical vapor infiltration (CVI) [9], and reactive melt infiltration (RMI) [10], in which the RMI process shows the obvious advantages of high densification efficiency and low cost, and is appealing in the manufacturing of low porosity composites with various geometries [11].

Up until now, numerous efforts have been devoted to infiltrating Si or Zr into CFC composites to prepare C/C–SiC or C/C–ZrC composites, respectively [12–16]. However,

due to the poor ablation resistance of C/C–SiC, and the weak oxidation resistance of C/C–ZrC, neither of them is suitable to use alone in hypersonic aircrafts. Some studies have demonstrated that infiltrating a Si–Zr alloy to modify CFC composites can simultaneously take advantage of SiC and ZrC ceramics [10]. The ZrO_2 skeleton generated by ZrC oxidation exhibits a high melting point (~2700 °C) and extremely low vapor pressure. The SiO_2 layer, produced from SiC oxidation, transits to a glassy state above 1175 °C and shows sluggish oxygen diffusion through it. The ZrO_2 skeleton is covered by a glassy SiO_2 layer, which can cooperatively inhibit the oxygen corrosion of the matrix [17]. Moreover, Si–Zr intermetallic compounds, which partially or completely replace residual Si, can further improve the working temperature limited by the Si softening. Tong et al. modified CFC preforms via RMI with a Si–Zr10 eutectic alloy below 1600 °C, but the enhancement in the ablation resistance of the as-fabricated C/C–SiC composites is finite because of a low ZrC content [18–20]. By infiltrating the $Si_{0.87}Zr_{0.13}$ alloy into porous CFC preforms at 1800 °C, Wang et al. obtained C/C–SiC–ZrC composites with a high strength, due to the gradient structure of the SiC–ZrC matrix [10]. Chen et al. firstly used carbon fabric to prepare C/B_4C–C preforms by sol-gel and SI, and then fabricated C/ZrC–ZrB_2–SiC composites after the infiltration of $ZrSi_2$ melt into the preforms at 1850 °C. They also investigated the effects of preform pore structure on infiltration kinetics [21]. As aforementioned, in order to introduce more ZrC or ZrB_2, hypereutectic Si–Zr alloys are mainly used as the infiltrant, which leads to very high temperatures (≥1800 °C) in the RMI process. However, such high temperatures will increase the uncontrollability during RMI, and eventually result in the following two problems: fiber erosion and infiltration channel chocking [22,23]. Lowering the temperatures of the RMI process can not only reduce the degradation of carbon fibers, but also decrease the cost of preparation.

Therefore, in this study, the C/C–SiC–ZrB_2 composites with a higher ZrB_2 content were expected to be fabricated at a relatively low temperature, by a combined process of SI and RMI. The porous C/C–B_4C and C/C–ZrB_2 preforms prepared by SI were infiltrated with the Si–Zr10 eutectic alloy at 1600 °C to achieve C/C–SiC–ZrB_2 composites. The SiC matrix was formed by the reaction between C and Si during the RMI process, while the ZrB_2 matrix was obtained by in situ generation from the reaction of B_4C and Si–Zr10 melt, or by direct introduction via ZrB_2 slurry impregnation. The effects of B_4C and ZrB_2 particles on the microstructural evolution of C/C–SiC–ZrB_2 composites were investigated, and the formation mechanism of the SiC–ZrB_2 matrix was summarized by schematic diagrams. This study provides guidance on the fabrication of C/C–SiC–ZrB_2 composites with a higher ZrB_2 content by Si–Zr alloy infiltration at a relatively mild temperature.

2. Materials and Methods

The fabrication procedure of C/C–SiC–ZrB_2 composites is schematically shown in Figure 1. The density and fiber volume of two-dimensional porous CFC skeletons prepared by CVI are 0.90 g/cm^3 and 17.6%, respectively. B_4C and ZrB_2 aqueous slurries were prepared as follows: the dispersant was firstly dissolved in deionized water, then B_4C powder (average particle size: 0.5 μm, purity: 99.5%; Bike Nano Technology Company, Shanghai, China) and ZrB_2 powder (average particle size: 0.7 μm, purity: 98.0%; China New Metal Materials Technology Co., Ltd, Beijing, China) were added into the dispersant solution, followed by planetary ball milling with ZrO_2 balls for 10 h. Subsequently, CFC skeletons were vacuum impregnated (VI) with B_4C slurry or ZrB_2 slurry, and dried at 120 °C. After repeating the above infiltration steps for three and seven cycles, C/C–B_4C and C/C–ZrB_2 preforms were obtained. Then, these two preforms were infiltrated by phenolic resin (THC-800, purity: 95.0%; Shaanxi Taihang Fire Retardant Polymer Co., Ltd., Xi'an, China) ethanol solution to supply carbon source and fix the boride particles, followed by pyrolysis at 1000 °C and thermal treatment at 1600 °C. Finally, C/C–SiC–ZrB_2 composites were produced in a vacuum furnace by infiltrating Si–Zr10 melt into the preforms at 1600 °C for 1 h. Here, the composite obtained from the C/C–B_4C preform is marked as B_4C-composite, and the other is marked as ZrB_2-composite.

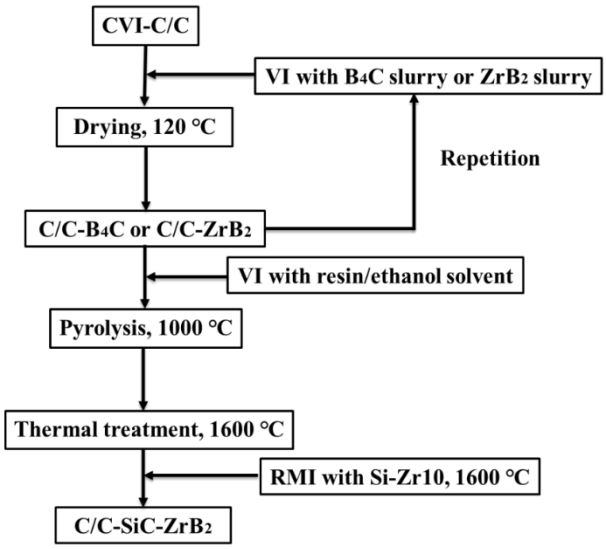

Figure 1. The fabrication procedure of C/C–SiC–ZrB_2 composites.

The density and open porosity were measured by Archimedes' method. The phase compositions were characterized by using X-ray diffraction (XRD, mode: X' PERT PRO MPD, PANalytical B.V., Almelo, Holland) from 5° to 90° (2θ) with Cu K_α radiation (λ = 1.54 Å, 40 KV, 40 mA). The phase volume fractions of the composites were estimated by X-ray fluorescence (XRF, mode: Axios, PANalytical B.V., Holland) of oxidized samples. The microstructures of different specimens were analyzed by scanning electron microscopy (SEM, mode: JSM-7001F, JEOL, Tokyo, Japan) and the elemental analysis was conducted by energy dispersive spectroscopy (EDS, mode: INCA X-MAX, Oxford Instruments, Abingdon, UK). The size distributions of ceramic particles were obtained from SEM images. At least 100 congener particles were selected from random areas to reduce the error of statistical analysis. The flexural strength of the samples with a dimension of 40.0 mm × 4.2 mm × 3.2 mm was measured by a three-bending test on universal testing machine (MTS, Mechanical Testing & Simulation, Eden Prairie, MN, USA), with a span of 30.0 mm and a loading rate of 0.5 mm/min.

3. Results and Discussion

3.1. Microstructural Characterization of the C/C–SiC–ZrB_2 Composites

The properties of the C/C–B_4C and C/C–ZrB_2 preforms are listed in Table 1. Owing to the lower density of B_4C (2.52 g/cm^3) when compared with ZrB_2 (6.1 g/cm^3), the B_4C slurry, with the same mass fraction as the ZrB_2 slurry, has relatively higher viscosity and larger flow resistance. Thus, the C/C–B_4C preform, with similar open porosity to the C/C–ZrB_2 preform, can be achieved after fewer cycles of B_4C slurry infiltration. Figure 2 displays the SEM images for the polished cross-sections of these two preforms. As shown in Figure 2a,c, both preforms show similar microstructures, and there are many scattered pores between the fiber bundles. The gaps in the concentrated areas of the fiber bundles are occupied by pyrolytic carbon layers with a thickness of ~6 μm, while the voids among the loose areas of the fiber bundles are filled with a B_4C–C or ZrB_2–C mixture. In addition, the micro-cracks observed in the B_4C–C and ZrB_2–C mixtures can provide infiltration channels for the Si–Zr10 alloy (Figure 2b,d).

Table 1. Properties of C/C–B_4C and C/C–ZrB_2 preforms before and after reactive melt infiltration (RMI).

Samples	Density (g/cm^3)	Open Porosity (%)	Phase Volume Fraction (%)				
			C_f	ZrB_2	B_4C	$ZrSi_2$	SiC
C/C-B_4C	1.27	32.07	17.60	N/A	6.74	N/A	N/A
C/C-ZrB_2	1.58	34.75	17.60	9.51	N/A	N/A	N/A
B_4C-composite	1.98	18.04	17.60	1.47	5.87	2.45	23.10
ZrB_2-composite	2.82	3.43	17.60	9.51	N/A	4.26	38.67

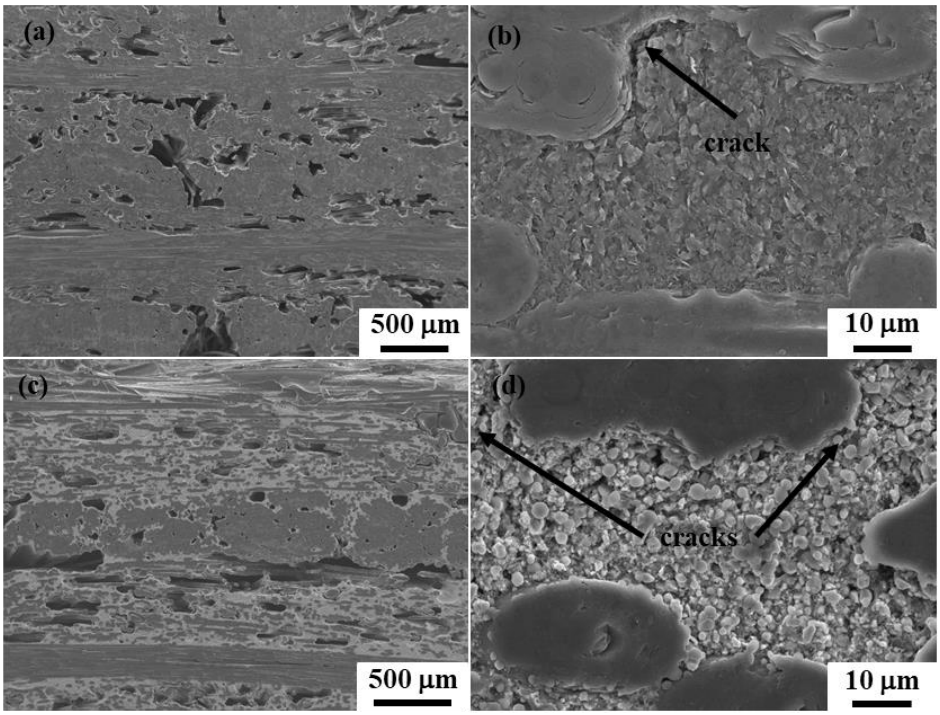

Figure 2. SEM images of several used preforms: polished cross-sections of porous C/C–B_4C (**a**) and C/C–ZrB_2 preforms (**c**); the B_4C–C (**b**) and ZrB_2–C mixture (**d**) between carbon fibers.

As demonstrated in Table 1, after infiltrating the Si–Zr10 alloy into the porous preforms, the density and open porosity of the as-fabricated B_4C-composite are 1.98 g/cm^3 and 18.04%, respectively, while those of the ZrB_2-composite are 2.82 g/cm^3 and 3.43%, respectively. The cross-sectional morphologies and detailed microstructures of the C/C–SiC–ZrB_2 composites are shown in Figure 3. The B_4C-composite shows a loose and porous structure, which is consistent with its low density (Figure 3a). The reasons for the loose structure of the B_4C-composite can be mainly concluded in the following two aspects: firstly, it is easy to form a dense B_4C layer near the surface of the C/C–B_4C preform during the SI process, on account of the higher solid content of the slurry; secondly, the SiC–ZrB_2 matrix formation reaction from the Si–Zr10 melt and B_4C–C is intensely exothermic, and the thermal expansion coefficients of ZrB_2 (6.2×10^{-6} K^{-1}) and SiC (4×10^{-6} K^{-1}) are higher than that of carbon (2–4 $\times 10^{-6}$ K^{-1}) [24,25]. The volume expansion caused by in situ generated SiC–ZrB_2 ceramics may further reduce, or even block, the infiltration channels of the melt. To further investigate the microstructure of B_4C-composite, EDS analysis was carried out at the compact region between the fiber bundles (Figure 3c,e,g). There is only a continuous SiC layer near the B_4C–C mixture, and some isolated ZrB_2 particles, less than 1 μm, are dispersed in the SiC ceramic, far away from the SiC layer. When close to the center of the matrix, tens of micron-sized irregular ZrB_2 particles are connected into a monolithic ZrB_2 ceramic, which suggests that the distributions of in situ synthesized SiC

and ZrB_2 are not uniform at a micro-scale level. Moreover, there are strip-shaped residual alloys with a composition that is close to $ZrSi_2$ in the center of the matrix.

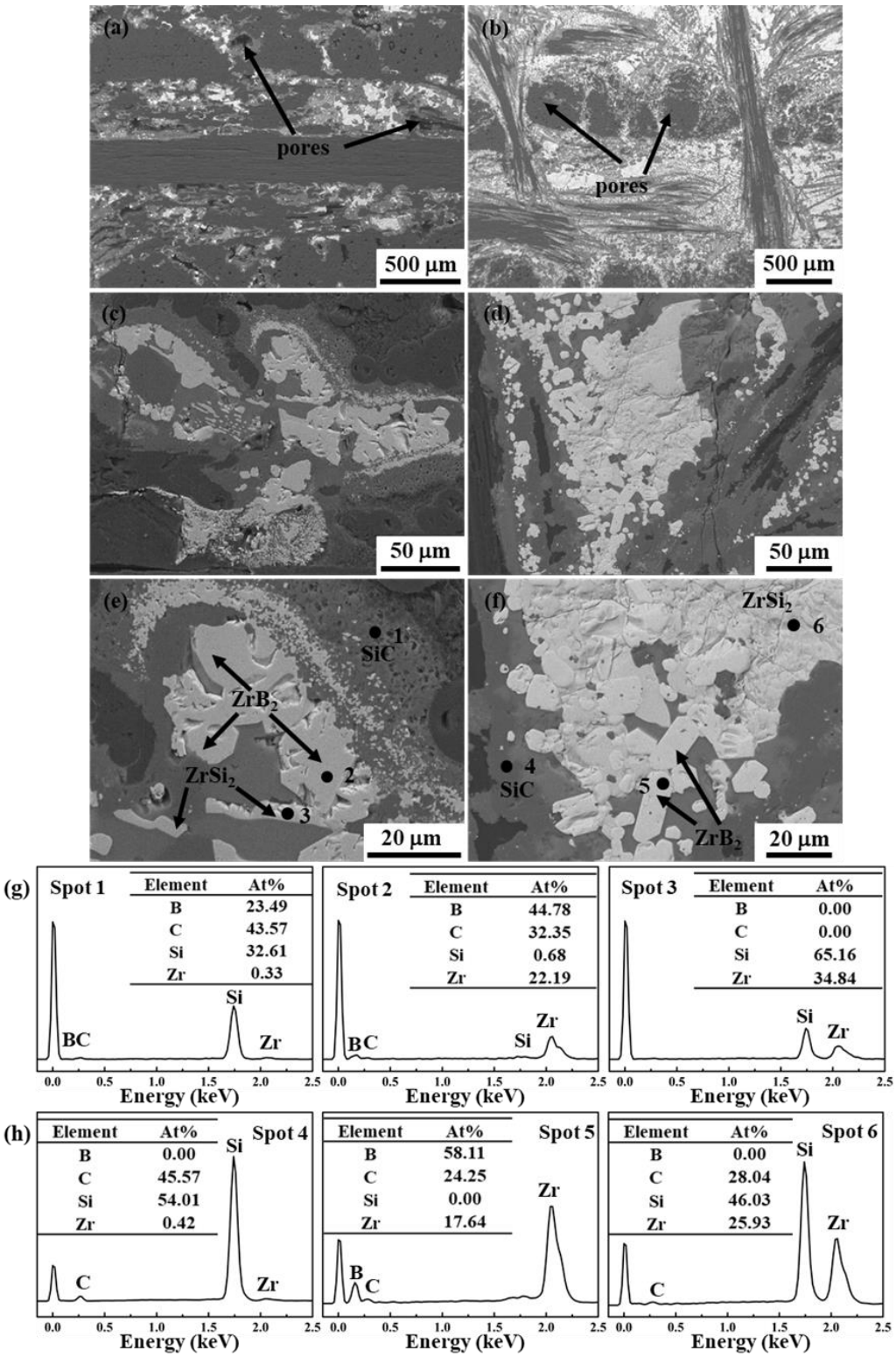

Figure 3. Back-scattering images and EDS analysis for polished cross-sections of C/C–SiC–ZrB_2 composites: (**a**,**c**,**e**,**g**) B_4C-composite; (**b**,**d**,**f**,**h**) ZrB_2-composite.

In contrast, the ZrB_2-composite presents a denser microstructure, where several closed micro-pores can only be observed in intra-bundle regions (Figure 3b). According to EDS

analysis (Figure 3f), the matrix in the ZrB_2-composite mainly consists of a continuous grey SiC phase, a white plate-like ZrB_2 phase, and a rough white bulk $ZrSi_2$ phase. Figure 3d further shows that the ZrB_2–C mixture successfully transforms into a SiC–ZrB_2 matrix after the RMI process. Compared with the B_4C-composite, a continuous SiC layer is also formed closest to the carbon matrix in the ZrB_2-composite, and plate-like ZrB_2 ceramics are more scattered (Figure 3d). The voids between the plate-like ZrB_2 particles are mostly filled with the generated SiC ceramic. Besides that, the bulk $ZrSi_2$ alloy is distributed along the region that is rich in ZrB_2 (Figure 3f). Figures 2d and 3f further show that, after infiltration, the number of ZrB_2 particles declines, but the size of them increases significantly. The particle size distributions of ZrB_2 powder in the C/C–ZrB_2 preform and ZrB_2-composite are shown in Figure 4. On the whole, ZrB_2 in the preform is near-spherical, and the average size of larger particles is about 1.91 ± 0.44 μm (Figures 2d and 4a), while, after RMI, most of them grow into elongated plate-like particles with an average size of 7.36 ± 3.98 μm in the long axis direction (Figures 3f and 4b).

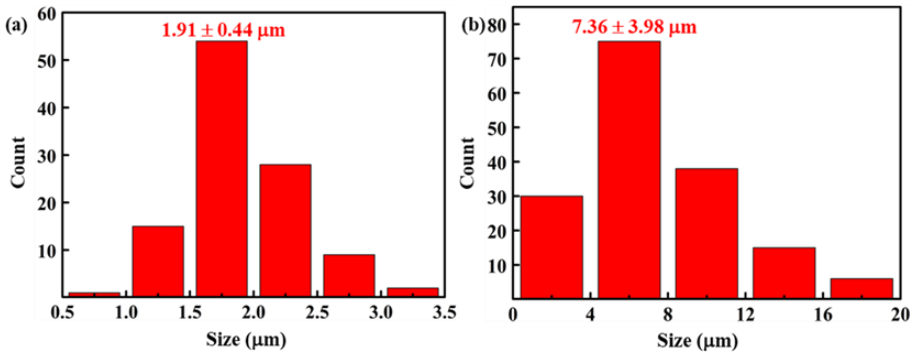

Figure 4. The particle size distributions of ZrB_2: (**a**) C/C–ZrB_2 preform; (**b**) ZrB_2-composite.

Figure 5 displays the XRD patterns of the C/C–B_4C and C/C–ZrB_2 preforms before and after the RMI process. The B_4C-composite consists of SiC, ZrB_2, residual $ZrSi_2$ alloy, unreacted B_4C, and amorphous C (Figure 5a). The result reveals that only the part of Zr in the Si–Zr10 alloy has been converted to ZrB_2, by reacting with B_4C, which conforms to the microscopic observation in Figure 3c and the low ZrB_2 content (1.47%) in Table 1. The diffraction peaks of the ZrB_2-composite mainly belong to the ZrB_2 and SiC phases (Figure 5b). In addition, residual Si, the $ZrSi_2$ phase, and a small amount of the ZrC phase are also detected. By analyzing the phase composition changes during the preparation procedure of the ZrB_2-composite, it is found that during the pyrolysis and carbonization of the phenolic resin at 1000 °C, slightly oxidized initial ZrB_2 particles are further oxidized to form m-ZrO_2. Then, ZrO_2 is turned into ZrC by carbothermal reduction with solid carbon in the process of heat treating at 1600 °C.

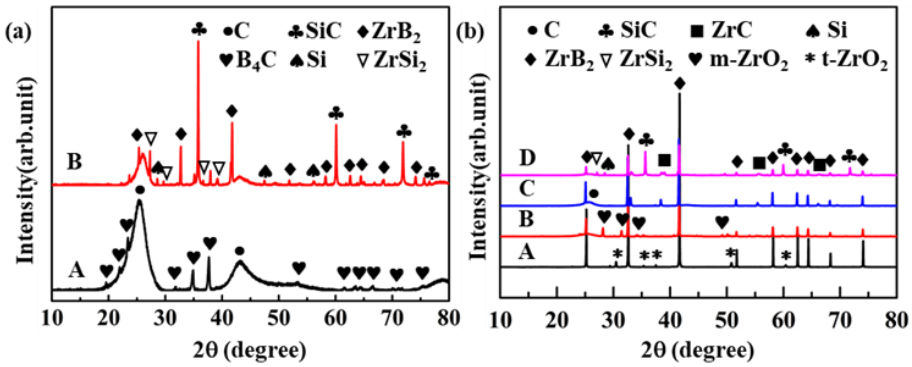

Figure 5. XRD patterns of different preforms and composites: (**a**) A, C/C–B_4C preform; B, B_4C-composite; (**b**) A, initial ZrB_2 particles; B, C/C–ZrB_2 preform after pyrolysis at 1000 °C; C, C/C–ZrB_2 preform after heat treating at 1600 °C; D, ZrB_2-composite.

3.2. Microstructural Evolution and Formation Mechanism of the C/C–SiC–ZrB_2 Composites

The target of preparing C/C–SiC–UHTC composites is to achieve a compact composite with a homogeneously distributed ceramic matrix and high UHTC content. Therefore, investigating the microstructural evolution and formation mechanism of C/C–SiC–ZrB_2 composites is conducive to optimizing the preparation conditions and improving the performance of the composites. In this work, the fabrication of C/C–SiC–ZrB_2 composites is mainly based on the following liquid–solid chemical reaction:

$$Si + C = SiC \tag{1}$$

$$Zr + C = ZrC \tag{2}$$

$$Zr + 2B = ZrB_2 \tag{3}$$

$$Zr + 2Si = ZrSi_2 \tag{4}$$

The Gibb's free energy change of these reactions, calculated by thermodynamics in the standard state, is shown as a function of temperature in Figure 6, which proves that each reaction is thermodynamically feasible. On the basis of microstructural characterization of the composites, their reaction ability, and the phase diagrams among the Si–Zr–C–B system, the microstructural evolution and formation mechanism of the SiC–ZrB_2 matrix is summarized in Figure 7.

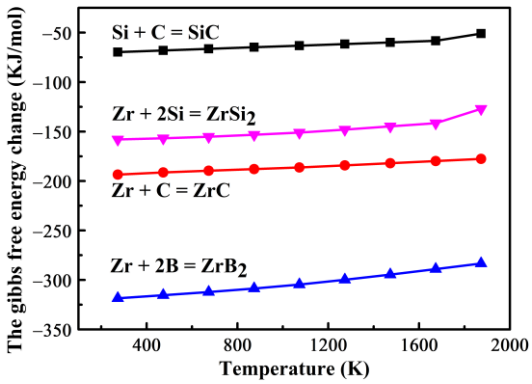

Figure 6. The Gibb's free energy change as a function of temperature for the reaction involved in this work.

As shown in Figure 7a, firstly, with the infiltration of molten Si–Zr10 into the C/C–B_4C preform, by capillary force, C and B atoms in the B_4C–C mixture dissolve into the alloy. Owing to the low Zr content in the Si–Zr10 eutectic alloy, the saturated solubility of C and B in the Si–Zr10 melt is close to that in pure Si melt. In terms of the Si–C and Si–B binary phase diagrams, the solubility of C is much lower than that of B in the Si melt at 1600 °C [26,27]. Thus, C atoms preferentially become saturated and react with enough Si, according to Equation (1), forming a continuous SiC layer. Then, the SiC layer separates the B_4C–C mixture from the melt, and the further formed SiC–ZrB_2 matrix is mainly controlled by the diffusion of C and B atoms through the layer [28]. Secondly, B atoms that can only be consumed by Zr atoms reach saturation. Figure 6 demonstrates that Equation (3) is more favorable than Equation (2) because of a more negative Gibb's free energy change, revealing that Zr prefers to react with B to form ZrB_2 via Equation (3). Therefore, the nucleation and precipitation of ZrB_2 grains occur in the melt. Thirdly, along with the continuation of the RMI process, the ZrB_2 grains coalesce and grow, forming a monolithic ZrB_2 ceramic. Finally, during the cooling process, with the gradual decrease in the saturated solubility of C and B atoms, the SiC and ZrB_2 ceramics further precipitate out, in which SiC is dominant because of a relatively higher Si content in the superfluous melt. Some ZrB_2 grains cannot migrate to the surface of the monolithic ZrB_2 ceramic in time, and become isolated particles in the SiC matrix [29]. In the areas far away from the B_4C–C mixture, since C and B atoms have

not diffused out, strip-shaped $ZrSi_2$ is generated via Equation (4) and separates out from the superfluous melt. Therefore, it can be concluded that the uneven SiC–ZrB_2 distribution in the B_4C-composite is primarily due to the asynchronous generation of SiC and ZrB_2 ceramics. In addition, the incomplete transformation from a Si–Zr10 alloy to a SiC–ZrB_2 matrix is attributed to the low diffusion coefficients of B and C atoms through the SiC layer.

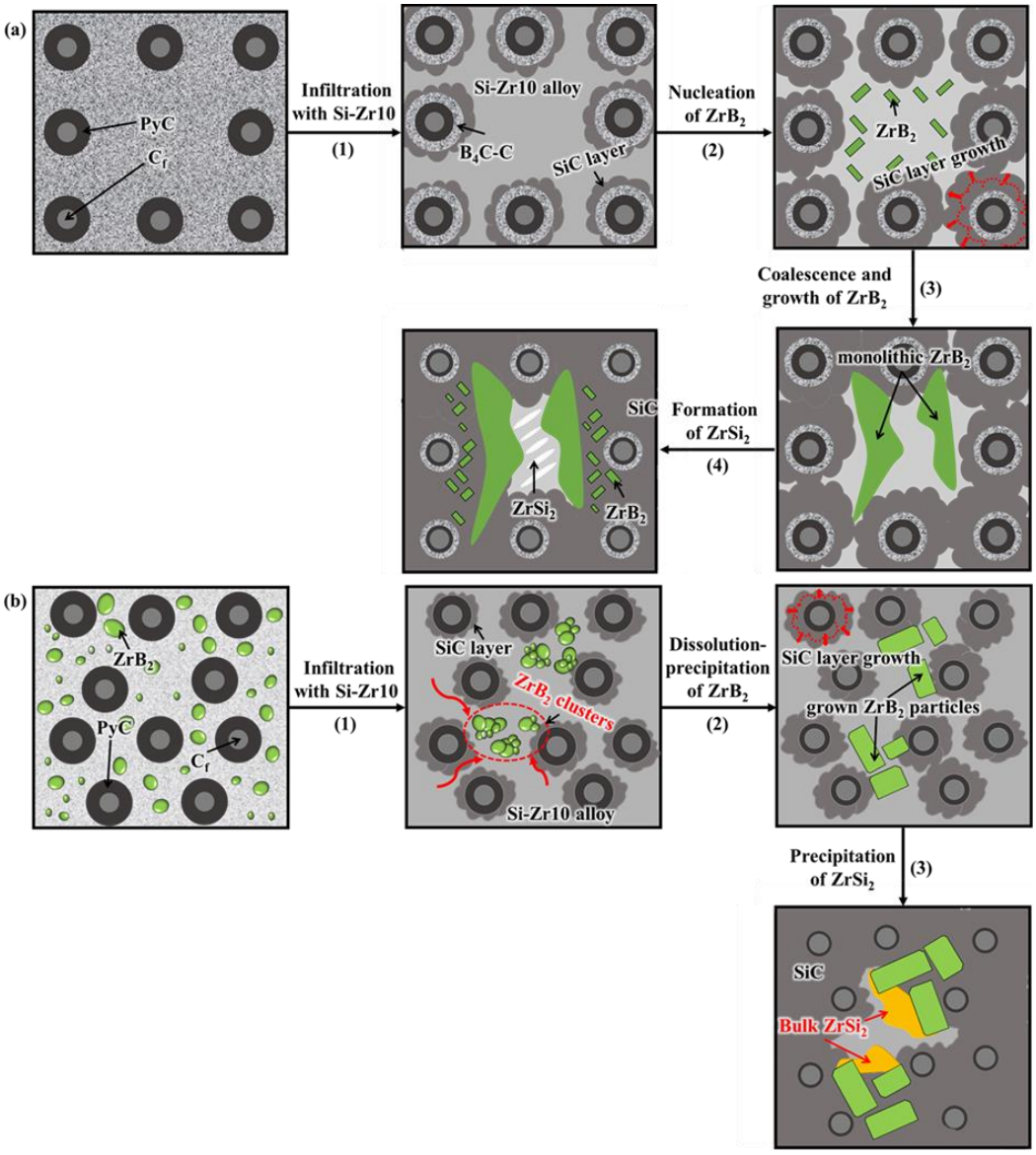

Figure 7. Schematic illustrations of microstructural evolution and formation mechanism for C/C–SiC–ZrB_2 composites during the RMI process: (**a**) B_4C-composite; (**b**) ZrB_2-composite.

Correspondingly, the structural evolution mechanism of the ZrB_2-composite is shown in Figure 7b. First, after infiltrating the molten Si–Zr10 alloy into the C/C–ZrB_2 preform, C atoms dissolve and become saturated quickly. A continuous layer, rich in SiC ceramic, is preferentially formed via Equation (1) because of the much higher Si content in the Si–Zr10 alloy. After that, the ZrB_2 particles, without the fixation of resin carbon, are rearranged and aggregated together to form larger clusters under the surface tension of the melt. As a previous study reported, ZrB_2 has highly covalent bonding and a low self-diffusion coefficient [30]. However, the liquid alloy between ZrB_2 particles with inhomogeneous sizes can accelerate mass transportation and facilitate grain boundary migration [31]. In addition, based on the phase diagrams of the Si–B and Si–Zr systems, B and Zr atoms have

certain solubility in liquid Si [27,32]. Considering the above four factors, the particles in ZrB_2 clusters grow through the dissolution–diffusion–precipitation mechanism. The small particles in each ZrB_2 aggregation dissolve and diffuse through the melt, then crystallize on the surface of large particles, leaving irregular gaps between the grown ZrB_2 particles. Moreover, previous studies have noted that the preferential growth directions of ZrB_2 grains are [210] and [110], which leads to the plate-shaped morphology of the grown ZrB_2 grains [33,34]. As the RMI process continues, a large amount of Si is consumed through Equation (1), and the composition of the melt shifts to hypereutectic, according to the Si–Zr phase diagram [32]. Meanwhile, the solid $ZrSi_2$ phase precipitates out from hypereutectic melt near the ZrB_2-rich areas due to the compatibility of the ZrB_2 and Zr elements. In summary, the introduction of ZrB_2 particles has no visible effect on the reaction process of infiltrating the Si–Zr10 alloy into CFC preforms. With the progress of infiltration, the composition of the Si–Zr10 eutectic alloy changes to hypereutectic, and bulk solid $ZrSi_2$ precipitates out. Besides that, the melt can accelerate the growth of ZrB_2 particles, which reduces the distribution uniformity of ZrB_2 ceramic in ZrB_2-composites.

3.3. Mechanical Properties of C/C–SiC–ZrB_2 Composite

According to a previous study on carbon fiber-reinforced ceramic matrix composites with the same fiber volume, the density of composites will be reduced with an increase in porosity, which leads to a sharp decrease in mechanical strength [35]. The ZrB_2-composite is believed to show better mechanical properties because it displays a denser matrix, along with much lower open porosity (3.43%) and much higher density (2.82 g/cm^3). Here, the mechanical property of the as-fabricated ZrB_2-composite was investigated by three-point bending tests. The flexural load–displacement curve and fracture surface micrograph are shown in Figure 8. The curve shows a step-like decline after reaching the maximum value (Figure 8a), proving that the ZrB_2-composite exhibits pseudo-plastic fracture behavior. The bending strength and elastic modulus are calculated to be 115.67 ± 8.85 MPa and 12.40 ± 1.90 GPa, respectively. Moreover, long fibers pull out and obvious interfacial debonding can be observed in Figure 8b, and the surface of the pulled-out fibers is relatively smooth, illustrating that most of the carbon fibers are not evidently eroded by the melt during the RMI process.

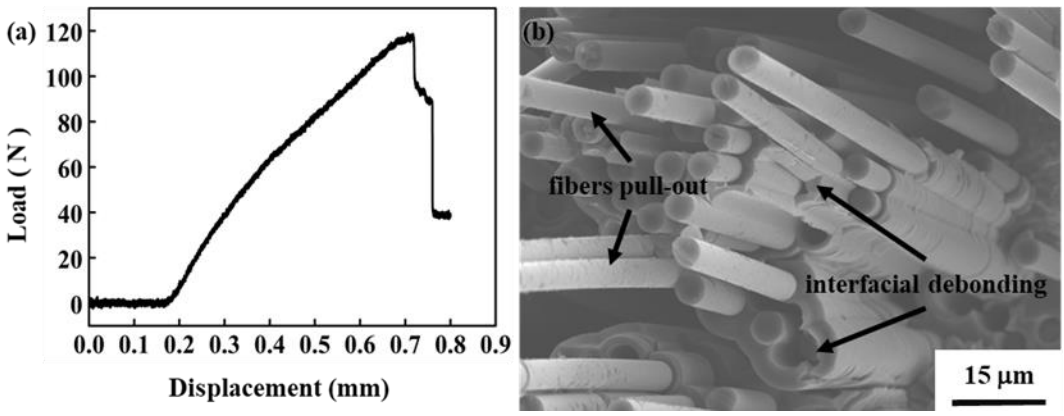

Figure 8. (**a**) Load–displacement curve of the ZrB_2-composites; (**b**) microstructure of fracture surface.

4. Conclusions

In summary, the C/C–SiC–ZrB_2 composites have been successfully fabricated by a combined process of SI and RMI through a Si–Zr10 eutectic alloy infiltration and chemical reaction at 1600 °C. Two preforms of C/C–B_4C and C/C–ZrB_2, with similar open porosities, were prepared through the SI process. Importantly, the effects of B_4C and ZrB_2 particles on the microstructural evolution and formation mechanism of C/C–SiC–ZrB_2 composites during RMI were explored. In the B_4C-composite, the ZrB_2 grains formed via

the reaction from B_4C particles and the Si–Zr10 melt coalesced together, and generated a monolithic ZrB_2 ceramic, which led to heterogeneous distribution of the SiC and ZrB_2 ceramics. In the ZrB_2-composite, the ZrB_2 particles were aggregated together to form clusters under the surface tension of the melt, and then grown into elongated plate-like particles through the dissolution–diffusion–precipitation mechanism. Compared with the B_4C-composite, the ZrB_2-composite had a higher ZrB_2 content (9.51%), higher density (2.82 g/cm^3), and lower open porosity (3.43%). Moreover, the ZrB_2-composite also exhibited pseudo-plastic fracture behavior, and most of the carbon fibers were not evidently eroded by the melt. Regrettably, resulting from the dissolution of resin carbon, the aggregation and growth of the ZrB_2 particles reduced the dispersion uniformity of the ZrB_2 ceramic in the ZrB_2-composite. This work not only provides a low-cost and relatively low-temperature strategy to fabricate C/C–SiC–ZrB_2 composites with a higher ZrB_2 content, through Si–Zr alloy infiltration, but also offers new insights into the effects of different boride particles on the liquid–solid reaction mechanism during the RMI process.

Author Contributions: Conceptualization, W.Z.; methodology, W.Z. and C.H.; validation, Q.S. and H.Z.; formal analysis, Q.S.; investigation, Q.S. and H.Z.; resources, C.H.; writing—original draft preparation, Q.S.; writing—review and editing, W.Z. and C.H.; project administration, W.Z. and C.H.; funding acquisition, W.Z. All authors have read and agreed to the published version of the manuscript.

Funding: This research was funded by Innovation Academy for Green Manufacture (Grant No. IAGM2020C22) and Key Laboratory of Multi-phase Complex Systems (Grant No. MPCS-2021-A-02), Chinese Academy of Sciences.

Conflicts of Interest: The authors declare no conflict of interest.

References

1. Fitzer, E. The future of carbon-carbon composites. *Carbon* **1987**, *25*, 163–190. [CrossRef]
2. Windhorst, T.; Blount, G. Carbon-carbon composites: A summary of recent developments and applications. *Mater. Des.* **1997**, *18*, 11–15. [CrossRef]
3. Li, T.; Yang, Z.; Qiao, S.; Zheng, X. High temperature oxidation resistance improvement of carbon-carbon composite. *Carbon* **1993**, *31*, 1361–1363. [CrossRef]
4. Liu, L.; Li, H.J.; Feng, W.; Shi, X.H.; Li, K.Z.; Guo, L.J. Ablation in different heat fluxes of C/C composites modified by ZrB_2–ZrC and ZrB_2–ZrC–SiC particles. *Corros. Sci.* **2013**, *74*, 159–167. [CrossRef]
5. Jin, X.C.; Fan, X.L.; Lu, C.S.; Wang, T.J. Advances in oxidation and ablation resistance of high and ultra-high temperature ceramics modified or coated carbon/carbon composites. *J. Eur. Ceram. Soc.* **2018**, *38*, 1–28. [CrossRef]
6. Arai, Y.; Inoue, R.; Goto, K.; Kogo, Y. Carbon fiber reinforced ultra-high temperature ceramic matrix composites: A review. *Ceram. Int.* **2019**, *45*, 14481–14489. [CrossRef]
7. Li, Q.G.; Dong, S.M.; Wang, Z.; He, P.; Zhou, H.J.; Yang, J.S.; Wu, B.; Hu, J.B. Fabrication and properties of 3D C_f/SiC–ZrC composites, using ZrC precursor and polycarbosilane. *J. Am. Ceram. Soc.* **2012**, *95*, 1216–1219. [CrossRef]
8. Zhou, H.J.; Ni, D.W.; He, P.; Yang, J.S.; Hu, J.B.; Dong, S.M. Ablation behavior of C/C-ZrC and C/SiC-ZrC composites fabricated by a joint process of slurry impregnation and chemical vapor infiltration. *Ceram. Int.* **2018**, *44*, 4777–4782. [CrossRef]
9. Tang, S.F.; Deng, J.Y.; Wang, S.J.; Liu, W.C. Fabrication and characterization of an ultra-high-temperature carbon fiber-reinforced ZrB_2–SiC matrix composite. *J. Am. Ceram. Soc.* **2007**, *90*, 3320–3322. [CrossRef]
10. Wang, Y.G.; Zhu, X.J.; Zhang, L.T.; Cheng, L.F. C/C-SiC-ZrC composites fabricated by reactive melt infiltration with $Si_{0.87}Zr_{0.13}$ alloy. *Ceram. Int.* **2012**, *38*, 4337–4343. [CrossRef]
11. Tang, S.F.; Hu, C.L. Design, preparation and properties of carbon fiber reinforced ultra-high temperature ceramic composites for aerospace applications: A review. *J. Mater. Sci. Technol.* **2017**, *33*, 117–130. [CrossRef]
12. Jiang, S.Z.; Xiang, X.; Chen, Z.K.; Xiao, P.; Huang, B.Y. Influence factors of C/C–SiC dual matrix composites prepared by reactive melt infiltration. *Mater. Des.* **2009**, *30*, 3738–3742. [CrossRef]
13. Zhong, Q.; Zhang, X.Y.; Dong, S.M.; Yang, J.S.; Hu, J.B.; Gao, L.; He, P.; Zhou, H.J.; Wang, Z.; Ding, Y.S. Reactive melt infiltrated C_f/SiC composites with robust matrix derived from novel engineered pyrolytic carbon structure. *Ceram. Int.* **2017**, *43*, 5832–5836. [CrossRef]
14. Guo, W.J.; Ye, Y.C.; Bai, S.X.; Zhu, L.A.; Li, S. Preparation and formation mechanism of C/C-SiC composites using polymer-Si slurry reactive melt infiltration. *Ceram. Int.* **2020**, *46*, 5586–5593. [CrossRef]
15. Zou, L.; Wali, N.; Yang, J.M.; Bansal, N.P.; Dong, Y. Microstructural characterization of a C_f/ZrC composite manufactured by reactive melt infiltration. *Int. J. Appl. Ceram. Technol.* **2011**, *8*, 329–341. [CrossRef]

16. Chen, S.A.; Zhang, C.R.; Zhang, Y.D.; Hu, H.F. Influence of pyrocarbon amount in C/C preform on the microstructure and properties of C/ZrC composites prepared via reactive melt infiltration. *Mater. Des.* **2014**, *58*, 570–576. [CrossRef]
17. Ju, L.; Lenosky, T.J. Thermochemical and mechanical stabilities of the oxide scale of ZrB_2+SiC and oxygen transport mechanisms. *J. Am. Ceram. Soc.* **2008**, *91*, 1475–1480. [CrossRef]
18. Tong, Y.G.; Bai, S.X.; Zhang, H.; Chen, K. C/C–SiC composite prepared by Si–10Zr alloyed melt infiltration. *Ceram. Int.* **2012**, *38*, 3301–3307. [CrossRef]
19. Tong, Y.G.; Bai, S.X.; Qin, Q.H.; Zhang, H.; Ye, Y.C. Effect of infiltration time on the microstructure and mechanical properties of C/C-SiC composite prepared by Si-Zr10 alloyed melt infiltration. *Ceram. Int.* **2015**, *41*, 4014–4020. [CrossRef]
20. Tong, Y.G.; Cai, Z.H.; Bai, S.X.; Hua, M.Y.; Xie, W.; Ye, Y.C.; Li, Y. Microstructures and properties of Si-Zr alloy based CMCs reinforced by various porous C/C performs. *Ceram. Int.* **2018**, *44*, 16577–16582. [CrossRef]
21. Chen, X.W.; Feng, Q.; Kan, Y.M.; Ni, D.W.; Zhou, H.J.; Gao, L.; Zhang, X.Y.; Ding, Y.S.; Dong, S.M. Effects of preform pore structure on infiltration kinetics and microstructure evolution of RMI-derived C_f/ZrC-ZrB_2-SiC composite. *J. Eur. Ceram. Soc.* **2020**, *40*, 2683–2690. [CrossRef]
22. Ni, D.W.; Wang, J.X.; Dong, S.M.; Chen, X.W.; Kan, Y.M.; Zhou, H.J.; Gao, L.; Zhang, X.Y. Fabrication and properties of C_f/ZrC-SiC-based composites by an improved reactive melt infiltration. *J. Am. Ceram. Soc.* **2018**, *101*, 3253–3258. [CrossRef]
23. Chiang, Y.-M.; Messner, R.P.; Terwilliger, C.D.; Behrendt, D.R. Reaction-formed silicon carbide. *Mater. Sci. Eng. A* **1991**, *144*, 63–74. [CrossRef]
24. Baxter, R.I.; Rawlings, R.D.; Iwashita, N.; Sawada, Y. Effect of chemical vapor infiltration on erosion and thermal properties of porous carbon/carbon composite thermal insulation. *Carbon* **2000**, *38*, 441–449. [CrossRef]
25. Fahrenholtz, W.G.; Hilmas, G.E.; Talmy, I.G.; Zaykoski, J.A. Refractory biborides of zirconium and hafnium. *J. Am. Ceram. Soc.* **2007**, *90*, 1347–1364. [CrossRef]
26. Durand, F.; Duby, J.C. Carbon solubility in solid and liquid silicon—A review with reference to eutectic equilibrium. *J. Phase Equilib.* **1999**, *20*, 61–63. [CrossRef]
27. Ikhmayies, S.J. Thermo-calc determination of phase diagram of Si-B binary system. *JOM* **2021**, *73*, 253–259. [CrossRef]
28. Zou, L.H.; Wali, N.; Yang, J.-M.; Bansal, N.P. Microstructural development of a C_f/ZrC composite manufactured by reactive melt infiltration. *J. Eur. Ceram. Soc.* **2010**, *30*, 1527–1535. [CrossRef]
29. Wang, D.K.; Dong, S.M.; Zhou, H.J.; Zhang, X.Y.; Ding, Y.S.; Zhu, G.X. Fabrication and microstructure of 3D C_f/ZrC-SiC composites: Through RMI method with ZrO_2 powders as pore-making agent. *Ceram. Int.* **2016**, *42*, 6720–6727. [CrossRef]
30. Sonber, J.K.; Suri, A.K. Synthesis and consolidation of zirconium diboride: Review. *Adv. Appl. Ceram.* **2011**, *11*, 321–334. [CrossRef]
31. Monteverde, F.; Bellosi, A.; Guicciardi, S. Processing and properties of zirconium diboride-based composites. *J. Eur. Ceram. Soc.* **2002**, *22*, 279–288. [CrossRef]
32. Bulanova, M.; Firstov, S.; Gornaya, I.; Miracle, D. The melting diagram of the Ti-corner of the Ti–Zr–Si system and mechanical properties of as-cast compositions. *J. Alloys Compd.* **2004**, *384*, 106–114. [CrossRef]
33. Otani, S.; Ishizawa, Y. Preparation of ZrB_2 single crystals by the floating zone method. *J. Cryst. Growth* **1996**, *165*, 319–322. [CrossRef]
34. Ji, Z.; Sun, S.K.; Zhang, G.J.; Kan, Y.M.; Wang, P.L.; Ohji, T. Chemical reactions, anisotropic grain growth and sintering mechanisms of self-reinforced ZrB_2–SiC doped with WC. *J. Am. Ceram. Soc.* **2011**, *94*, 1575–1583. [CrossRef]
35. Xu, Y.; Zhang, L.; Cheng, L.; Yan, D. Microstructure and mechanical properties of three-dimensional carbon/silicon carbide composites fabricated by chemical vapor infiltration. *Carbon* **1998**, *36*, 1051–1056. [CrossRef]